Titre: Title:	Experimental methods in chemical engineering: X-ray fluorescence - XRF
Auteurs: Authors:	Mario Ferreiro González, Nooshin Saadatkhah, & Gregory Scott Patience
Date:	2024
Type:	Article de revue / Article
Référence: Citation:	González, M. F., Saadatkhah, N., & Patience, G. S. (2024). Experimental methods in chemical engineering: X-ray fluorescence - XRF. The Canadian Journal of Chemical Engineering, 25218 (15 pages). https://doi.org/10.1002/cjce.25218

Titre de la revue: Journal Title:	The Canadian Journal of Chemical Engineering
Maison d'édition: Publisher:	Wiley
URL officiel: Official URL:	https://doi.org/10.1002/cjce.25218
Mention légale: Legal notice:	

Received: 18 December 2023 | Revised: 27 January 2024 | Accepted: 29 January 2024

DOI: 10.1002/cjce.25218

THE CANADIAN JOURNAL OF CHEMICAL ENGINEERING

MINI REVIEW

Experimental methods in chemical engineering: X-ray fluorescence—XRF

Mario Ferreiro González | **Nooshin Saadatkhah** | **Gregory S. Patience**

Chemical Engineering, Polytechnique Montréal, Montréal, Québec, Canada

Correspondence
Gregory S. Patience, Chemical Engineering, Polytechnique Montréal, C.P. 6079, Succ. "CV", Montréal, H3C 3A7 QC, Canada.
Email: gregory-s.patience@polymtl.ca

Abstract

X-ray fluorescence (XRF) is a non-destructive spectrometric technique to detect elements with an atomic number from 11 (sodium) and beyond 92 (uranium). When X-rays or gamma rays eject tightly bound inner core electrons, an electron from an outer shell will fill the empty orbital and fluoresce. Every element has a characteristic fluorescence, which depends on the element and the electrons in the orbitals that are ejected and those that fill the orbital. With the characteristic energy of the fluorescence, we determine elemental composition and concentration when adequately calibrated. Typical run times range from a second to a few minutes with an sensitivity to as low as 1 μg g^{-1} (ppm). XRF guns are portable devices that produce qualitative data while libraries loaded to laboratory instruments are capable of producing quantitative data. A broad range of scientists and engineers apply XRF in research—140 of the 250 scientific categories in the Web of Science (WoS) cite XRF analyses. Of the 10,000 articles indexed in WoS since 2018, chemical engineering ranks fifth with the most articles. The focus of the research in this category includes adsorption and waste water, combustion and pyrolysis, catalysis and zeolites, and nanoparticles and oxidation.

KEYWORDS

elemental analysis, fluorescence, non-destructive, polymers, spectroscopy, WEEE, X-ray, XRF

1 | INTRODUCTION

X-ray fluorescence (XRF) determines the chemical composition of solids, liquids, and powders, together with their thickness and the composition of overlapping layers as in coatings. This method is fast and non-destructive with a concentration range from >1 μg g^{-1} (ppm) to 100%. The measurement and analysis time depends on the number of elements and accuracy required, and varies between seconds to an hour. The detection range is higher for elements with higher atomic numbers. Application of XRF includes metal, cement, oil, polymer, plastic and food industry, mining, mineralogy, geology, water and waste materials, and pharmacy.

In 1895, Rontgen discovered X-rays when he saw cathode rays (an incandescent green light) pass through a glass tube and project onto a fluorescent screen.[1,2] Roentgen named them X, meaning unknown. The discovery of X-rays initiated the theory of the atomic structure that was further developed after Thomson

introduced electrons in 1897.[3] Thomson directed cathode rays between two aluminium plates in a vacuum tube to observe luminescence on a glass at the end of the tube. The rays travelled downwards along the tube when the upper plate was negatively charged, and travelled upward when it was positively charged. They concluded that cathode rays were negatively charged particles (electrons).[4] In 1909, Barkla correlated the X-rays radiating from a sample to its atomic weight.[5] Coolidge with 20 other research chemists and a large body of assistants produced ductile tungsten (filament) by reducing impurities in 1910.[6] In 1913, Moseley developed the primary XRF theory by numbering elements. Moseley revised the periodic tables from atomic weight to atomic number and proved the relationship between frequency (energy) and the atomic number (Moseley's Law), which is the principle of X-ray spectrometry.[7] He observed in an X-ray spectrum that the K line transitions moved the same amount each time the atomic number increased by one.[8] In 1925, Coster and Nishina were the first to use primary X-rays instead of electrons to excite a sample.[9] After that, Glocker and Schreiber were the first to quantitatively analyze materials with XRF.[10] Detector technology had to catch up in order to make the technique practical, which began after the 1940s. The 1950s saw the first commercially produced X-ray spectrometers. In 1970, the lithium drifted silicon detector was developed, which is still in use today.

XRF belongs mostly to the domain of material scientists and spectroscopy, as these two fields account for 25% of the >16,000 articles Web of Science (WoS) has indexed. Chemical engineers have contributed >1100.[11] The first article in the database was from 1967, and it took almost 30 years to reach 100 articles per year. In 2018, another 20 years later, WoS logged 1000 articles in a year. XRF is related to X-ray photoelectron spectroscopy (XPS),[12], X-ray diffraction (XRD),[13] and inductively coupled plasma (ICP) as it identifies and assesses the elemental composition and oxidation state. In terms of performance, it assesses bulk properties somewhat like XRD and Fourier transform infrared spectroscopy (FTIR), but the latter two report structural information.[14] XRF detects concentrations to less than 1 ppm while XRD is rarely capable of detecting species below 1% and FTIR goes to 100 ppm. This article belongs to a series on experimental methods and instrumentation most often applied by chemical engineers, which already includes such techniques as Raman, XPS, and XRD.[15] Instrumentation technology continues to advance in terms of both spatial resolution and detection limits of the elemental composition (Figure 1). XRF is a bulk technique with a lower detection limit compared to XRD and FTIR but analyzes over a larger area. μ-XRF, on the other hand, overlaps more with XPS and Raman as it samples a much smaller area (on the order of 10–100 μm) but it

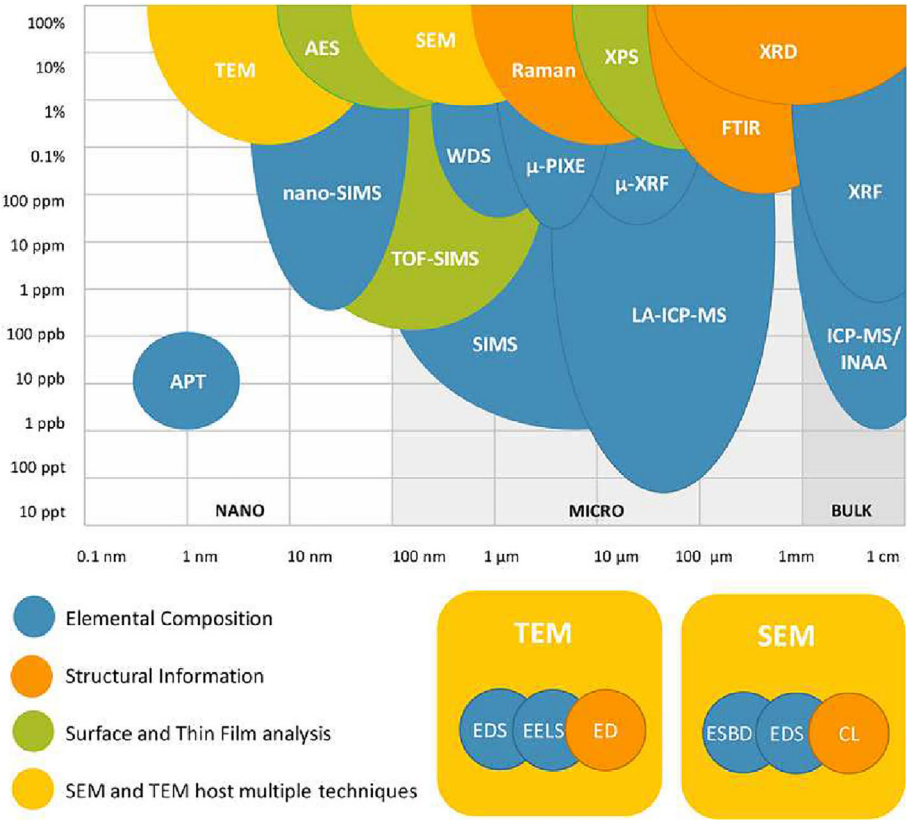

FIGURE 1 Diagram of microanalytical methods arranged according to spatial resolution and chemical sensitivity. AES, Auger electron spectroscopy. APT, atom-probe tomography. FTIR, Fourier transform infrared spectroscopy. ICP-MS/INAA, inductively coupled plasma mass spectrometry and instrumental neutron activation analysis. LA-ICP-MS, laser ablation inductively coupled mass spectrometry. μ-PIXE, micro particle-induced X-ray emission. SEM, scanning electron microscopy. TEM, transmission electron microscopy. TOF-SIMS, time-of-flight secondary ion mass spectroscopy. WDS, wavelength dispersive spectroscopy. XPS, X-ray photoelectron spectroscopy. XRD, X-ray diffraction. μ-XRF, micro X-ray fluorescence. (Copied from the work of Braidy et al.,[16] which was adapted from https://myscope.training/legacy/analysis/introduction/.)

detects elements with a sensitivity three orders of magnitude greater.

The target audience for the series includes students and experienced engineers that are less familiar with the specifics of each analytical instrument. Thus, we cover the theory and equipment only briefly but detail the applications and the limitations of the instrument—detection limits, repeatability, and uncertainty.

2 | THEORY

X-ray sources that irradiate samples include X-ray tubes, synchrotrons (an enormous particle accelerator that measures several kilometres in diameter), and radioactive material. X-rays were described as electromagnetic waves or beams of photons with a wavelength (or energy) between gamma-rays and ultraviolet light: 0.01–10 nm (or 0.125–125 keV).

XRF instruments bombard samples with X-ray radiation to remove electrons from the inner orbitals via the Compton or photoelectric effect—when the electron absorbs all of the photon energy, whereas in the Compton effect only part of the energy is taken by the electron. (Figure 2).

Once the the electron is ejected, other electrons from an outer orbital fill the empty space almost instantaneously (1×10^{-15} s). Due to the quantum nature of these interactions (when an electron absorbs or releases energy, it is a fixed amount of energy—photon—that depends on the atomic element and the transition), the transition to a lower energy state releases an element-specific energy, in this case, in the form of X-rays (fluorescence photon) that are measured by a detector. The element-specific fluorescence wavelength permits a qualitative determination while the intensity of the emission provides a quantitative analysis. The characteristic energy depends on the orbital from which the electron is removed and the filling electron orbital (Figure 3).

TABLE 1 K and L shell emission lines in keV.

Element	$K\alpha_1$	$K\alpha_2$	$K\beta_1$	$L\alpha_1$	$L\alpha_2$	$K\beta_1$
Br	11.92	11.87	13.29	1.48	1.48	1.52
Sb	26.35	26.11	29.72	3.60	3.59	3.84
Ti	4.51	4.50	4.93	0.45	0.45	0.48
Fe	6.40	6.39	7.057	0.70	0.70	0.71

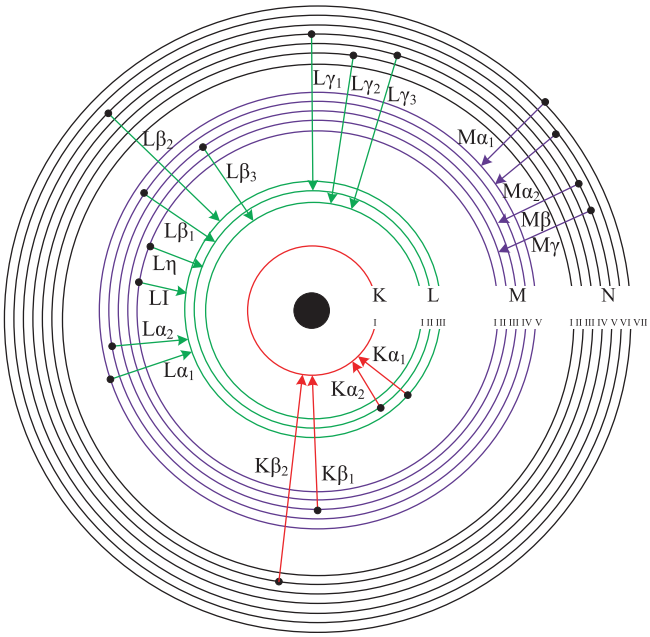

FIGURE 3 Not all transitions are permitted due to quantum reasons. The characteristic emission energy depends on the line and transition (Tables 1 and 2). Each line represent a different quantum coordinate (quantum number) of the expelled electron and the filling one. L lines for example represent the electrons situated on the energy level 2 and with defined n, l, m, and j values. For example, $K\alpha_1$ represents the transition from L3 to a K line.[17]

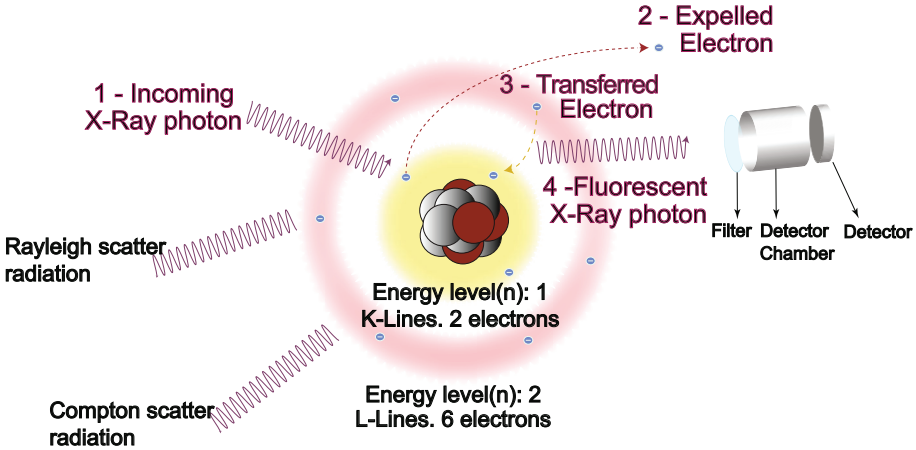

FIGURE 2 X-ray fluorescence (XRF) basics. When an X-ray photon collides and expels an electron from an inner shell, it leaves a hole in the shell. To recover nuclear stability, an electron from an outer shell drops into the lower shell to fill the hole. The drop from outer (higher energy) to inner layer (lower energy) fluoresces and each element/shell has a characteristic emission of this energy difference. Compton and Rayleigh scattering also result when an electron is ejected.

However, when a sample is bombarded with X-rays, it not only fluoresces, but it also produces an electron cascade (partially due to the Auger effect), bremsstrahlung X-rays (X-rays emitted when a charged particle "decelerates"), and backscattered X-rays (characteristic or fluorescence X-ray emission from underlying materials like air).[18,19]

Irradiating an atom with X-ray photons expels an electron with an energy level characteristic of the shell—L, K, M (and element). The atom that expels an electron leaves an empty orbital (initial vacancy) that places it in an unstable excited state (Figure 3). Siegbahn nomenclature follows the electron transition. For transitions from $n=2$ to $n=1$, the corresponding letter will be K; from $n=3$ to $n=2$, it is L; from $n=4$ to $n=3$ it is M; and so on (Table 2).

The emitted X-rays appear as peaks over a given energy spectrum (Figure 4). The intensity of each peak reflects the concentration of an element in the sample compared to regression line standards (Figure 5). Fluorescence and scatter depends on both the X-ray energy and the material characteristics (thickness, density, and composition).

Additionally to electronic transitions, the light–matter interaction and how the latter deposit energy in the former will dictate other parameters in XRF analysis such as penetration and analysis depth. This is not only relevant to perform elemental studies but also when talking about radiation exposure and safety. A beam of photons passing through an element will lose its energy proportionally to their initial intensity, material depth, and density.[20] This effect is defined as the mass attenuation coefficient (μ/ρ), and is proportional to is Avogadro's number, N_A and the sum of the principal photon interactions, σ_{tot}, and inversely proportional to the atomic mass unit, μ, and the relative atomic mass of a determined element, A.

$$\mu/\rho = \frac{\sigma_{tot} N_A}{\mu A} \quad (1)$$

where

$$\sigma_{tot} = \sigma_{pe} + \sigma_{coh} + \sigma_{incoh} + \sigma_{pair} + \sigma_{trip} + \sigma_{ph.n.} \quad (2)$$

and

- σ_{pe} photoelectric effect contribution
- σ_{coh} coherent scattering contribution
- σ_{incoh} incoherent scattering contribution
- σ_{pair} electron-positron production contribution
- σ_{trip} atomic electrons contribution
- $\sigma_{ph.n.}$ photonuclear contribution

Some of these contributions, like $\sigma_{ph.n.}$ and σ_{pair}, only occur at very high energies over 5 MeV. However, the attenuation coefficient, photon interaction cross sections, and related quantities depend on the photon energy.[20]

2.1 | Rayleigh and Compton scatter

In addition to XRF, elastic and inelastic interactions produce scattered photons. When a photon interacts in elastically with an electron, part of the photon energy transfers to the electron. The scattered photon will have a lower energy and therefore longer wavelength than the incoming photon and is known as Compton scatter or incoherent scatter. The energy lost by the photon depends of the collision angle.

Notation	n	l	m	$j=l\pm1/2$
K	1	0	0	1/2
L1, L2, L3	2	0, 1	0, 1, −1	1/2, 1/2, 3/2
M1, M2, M3, M4, M5	3	0, 1, 2	0, 1, −1, 2, −2	1/2, −1/2, 3/2, −3/2, 5/2

TABLE 2 A compilation of the possible quantum number for the first three energy levels of an atom and its correspondence with (n is the energy levels, l is angular quantum number, m is the magnetic quantum number).

TABLE 3 Operational parameters for all detectable elements applied to the brominated polymer.

Run	Element lines		V	I		
Omnian	K lines	L lines	kV	μA	Filter	He
5	F–Si		5	60	None	Yes
4	P–Cl		9	30	Ti	Yes
3	K–V	Te–Ba	12	25	Al, 50 μm	No
2	Cr–Co	Pr–Tm	20	15	Al, 200 μm	No
0	Ni–Mo	Yb–Am	50	6	Ag	No
1	Tc–Sb		50	6	Cu, 500 μm	No

The intensity of the scattered radiation is inversely proportional to the mass attenuation coefficient of an element (Figure 6). The mass attenuation factor is the ratio of the linear attenuation coefficient, measured in cm^{-1} μ, to the material density in g mL^{-1}, ρ. By measuring the mass attenuation coefficient of different elements, it is possible to use the Compton effect for quantitative analysis.[21]

$$\lambda = \frac{h}{m_e c}(1 - \cos\theta) \quad (3)$$

where:

$\Delta\lambda$ is the change in wavelength (Compton shift),
h is Planck's constant (6.63×10^{-34} J s^{-1}),
m_e is the electron mass,
c is the speed of light (3×10^8 m s^{-1}), and
θ is the scattering angle.

Strongly bound electrons resonate at the same frequency as incident photons and then emit scattered photons at that frequency—elastic scattering. This is known as Rayleigh or coherent scattering and the energy loss in the process approaches zero as photons scatter with the same energy as the incident photons.[21,22]

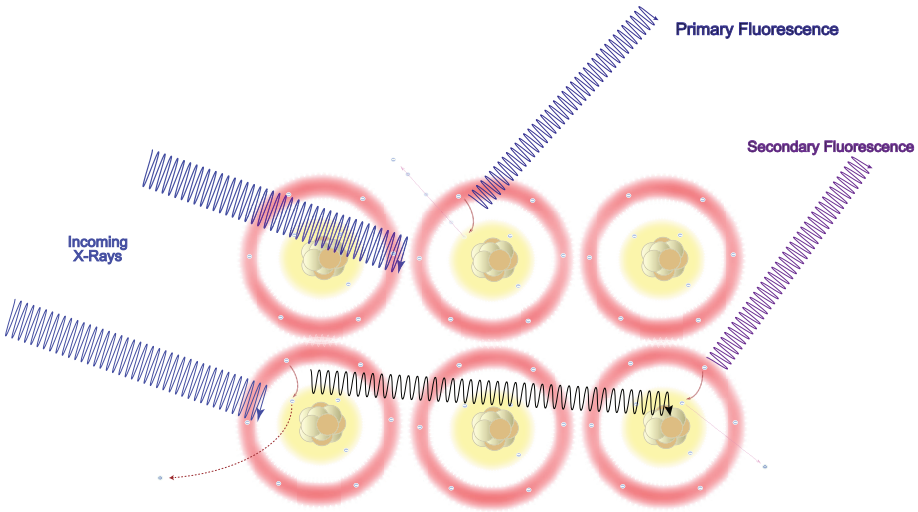

FIGURE 4 Primary fluorescence is the one directly induced by the X-ray source. Secondary fluorescence is created by the fluorescence X-ray from the sample itself acting as an X-ray source.

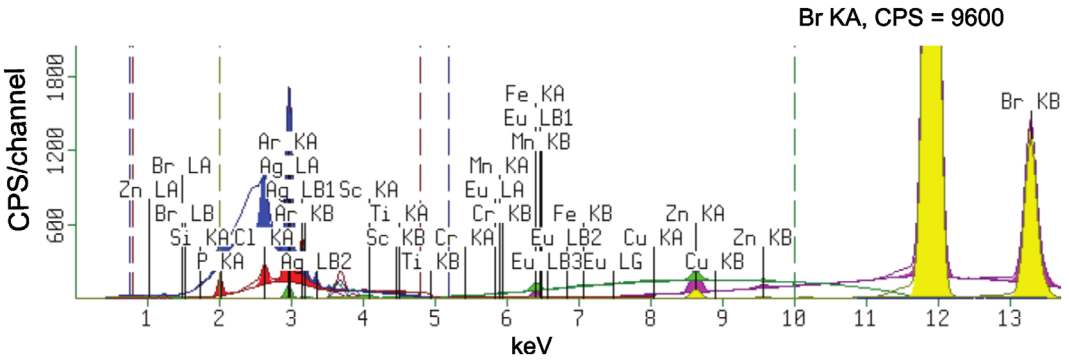

FIGURE 5 Standard X-ray fluorescence (XRF) trace for a plastic sample containing brominated fire retardant. The *y*-axis represents the number of counts (counts per second [CPS]) of light (X-ray photons) accumulated per detector channel. Each channel represents an energy range (keV). The *x*-axis represents the energy of the detected photon, in kilo electron volts (keV). The CPS is proportional to the element concentration, thus higher CPS means higher concentrations. If the resolution is high the peak will narrow the energy's value (*x*-axis) of the element's characteristic energy (Table 2, Figure 3). XRF spectrum details elements and transitions. The most noticeable peak corresponds to Br Kα_1 with 9600 counts while the second peak with the most counts was Br Kβ_1. In this case, Br is the element whereas Kα_1, Kβ_1 are the transitions. Zn Kα_1 is also well defined. Many element's traces are present and several overlap that have similar characteristics energies. The colour of the different peaks refer to the measuring conditions, who are optimized for a certain range of elements. In this case, using an Epsilon 4 from Malvern Panalytical coupled with Omnian Scan Parameters (Table 3). The yellow configuration is set to detect elements from Ni to Mo using K lines, and Yb to Am with L lines. The instrument applies a voltage of 50 kV and 6 μA to generate the X-rays. Additionally, this method use Ag filter and air atmosphere (for lighter elements, it is possible to use He).

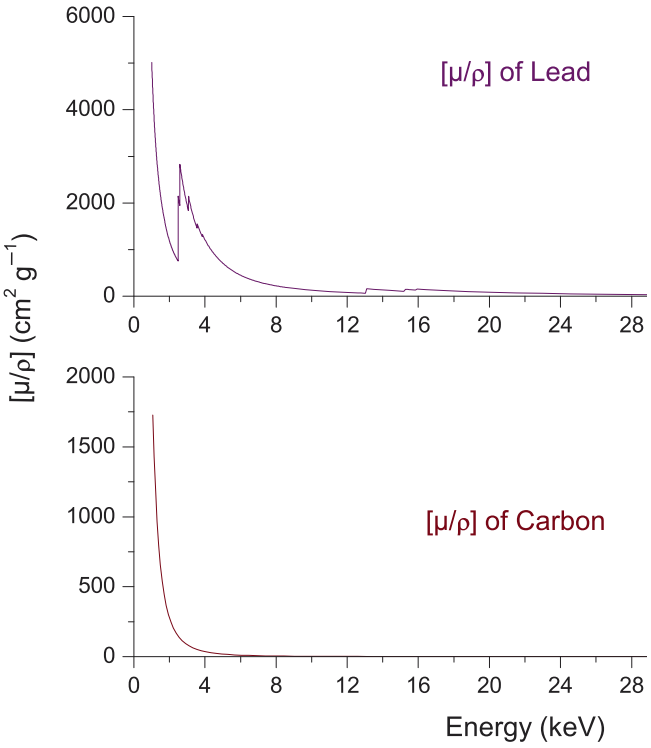

FIGURE 6 Mass attenuation (μ/ρ) for C (light element) and Pb (heavy element) and its variation with the incident radiation energy.

2.2 | Polarization

X-rays, as any electromagnetic wave, are transversal and thus the wave is perpendicular to the direction of transmission. They have both an electrical (E) and a magnetic component (B). A filter that polarizes X-rays rotates only one component of the electrical field (E). The polarization effect contemplated here affect both components, but in the explanation, we are considering only the electric component (E). When a wave is polarized, it means that all the electrical components of E are in the same plane.

Any electrical component of the electromagnetic wave is the vectorial sum of its horizontal and vertical components (E_z and E_x) (Figure 7). When non-polarized X-rays are reflected at a 90° angle, the resulting X-rays are polarized because the vertical components are not reflected in the new direction of propagation. Adding a second 90° reflection will eliminate all the original X-rays and thus reduce the background noise and improve the quality of the signal. Secondary targets are partially used for this purpose.

2.3 | X-ray tubes

X-ray tubes includes a filament (cathode) and an anode in a vacuum chamber (Figure 8).[23] An electrical current

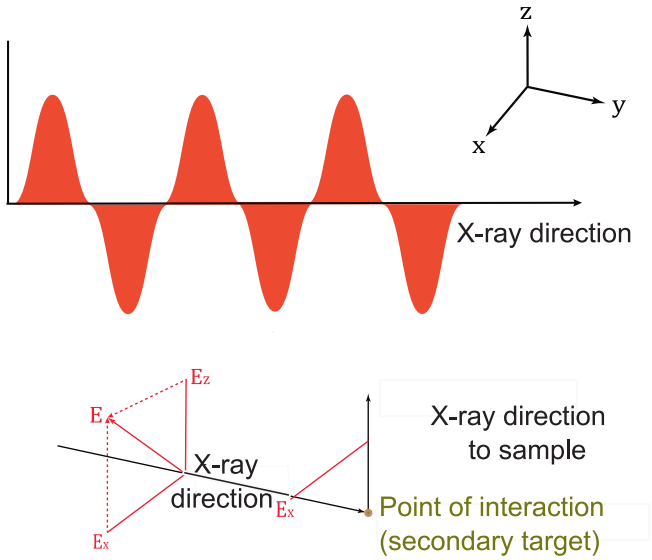

FIGURE 7 Polarization: As electromagnetic waves travel, the electrical component of the wave is perpendicular to direction of the motion. When the wave diffracts at 90°, the electrical component that was perpendicular and disappears. Repeating this operation two times removes the background.

heats up the filament, which then emits electrons. A high voltage (20–150 kV) across the filament and the anode accelerates electrons to the anodes.[24] Electrons hit the anode and decelerate, which makes the anode emit characteristic radiation (X-rays) and bremsstrahlung radiation in a continuous spectrum of energy (continuum). The energy of this radiation depends on the anode material (gadolinium, tungsten, rhenium, molybdenum, aluminium, chromium, palladium, gold, and graphite). Tungsten, because of its high atomic number ($Z = 74$), produces bremsstrahlung radiation more efficiently compared to other target materials with lower atomic number.[25] Molybdenum ($Z = 42$) and rhodium ($Z = 45$) with intermediate atomic number produce characteristic X-rays with intermediate energies for medical purposes.[26] Detection of light elements requires a high intensity of low energy radiation (1–10 keV), while heavy elements require excitation energies up to 50 keV (Figure 9).[27]

X-rays leave the end of the tube through a beryllium window or through side-windows (Figure 8).[28]

2.4 | Secondary targets

X-rays illuminate secondary targets (fluorescent, Barkla, and Bragg) producing characteristic radiation to irradiate samples. Secondary targets have multiple advantages; they (Figure 10): (1) polarize the radiation; (2) reduce or remove background noise; (3) generate specific emission

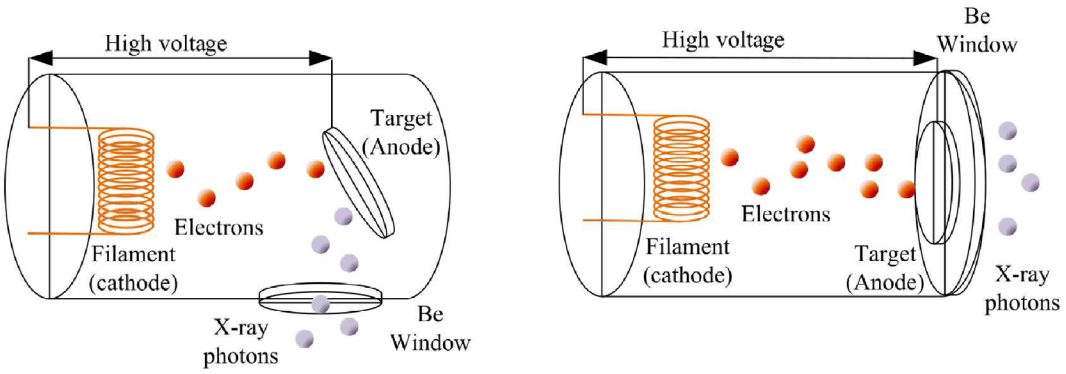

FIGURE 8 X-ray tube arrangement: Side window (left), target transmission (right).

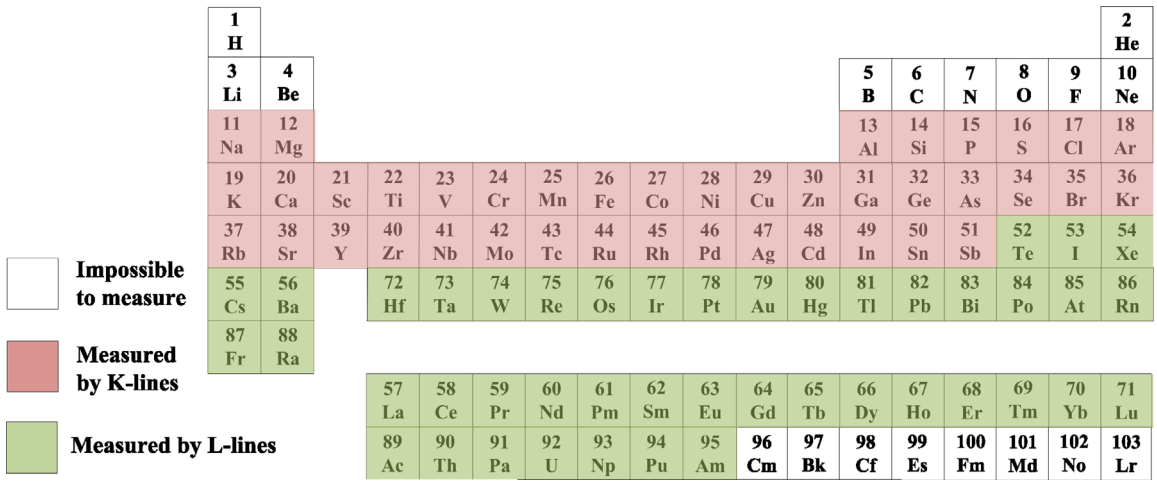

FIGURE 9 The measurability of the elements.

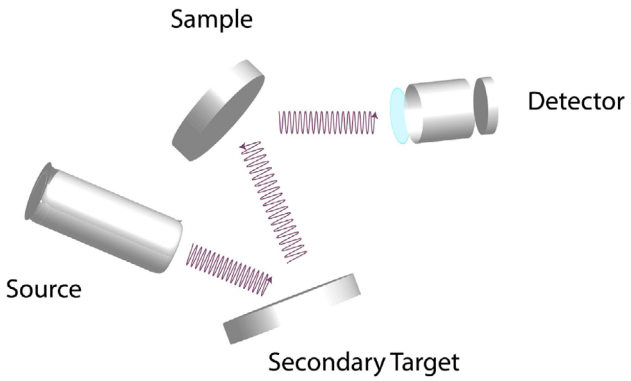

FIGURE 10 Secondary target configuration.

spectrum; (4) produce a wider energy distribution of the irradiating photons; and (5) improve detection limits.

Fluorescent targets include heavy elements like tungsten that fluoresce when irradiated by an X-ray source. Scattering is reduced but the the energy of the fluorescent radiation of the target must be greater than the bond energy of the electrons of the sample. Some instruments are equipped with several secondary targets allowing the selection of the desire fluorescent emission. **Barkla targets** consist of light elements to scatter photons. Some of the targets fluoresce, but the intensity is lower than the bond energy of the electrons of the sample. Barkla targets produce a wide energy spectrum and are best for heavy elements. **Bragg targets** are generally crystals that selectively reflect a specific energy in a desired direction, which improves the detection limits by reducing background levels.

2.4.1 | Detectors

XFR spectrometers comprise either energy dispersive (EDXRF) or wavelength dispersive (WDXRF) detectors. The former measures the energy of the characteristic radiation from the sample and separates it into elements in the sample (dispersion). The latter disperses the wavelengths by channelling all the radiation from the sample to crystal, like a prism, that diffracts the energies in several directions. EDXRF operates with a fraction of a Watt

with high detection efficiencies while WDXRF requires several kilowatts.[29] Ultimately, the energy of the electromagnetic wave, E, and wavelength, λ, are equivalent

$$E = hf = \frac{hc}{\lambda} \quad (4)$$

EDXRF has solid-state detectors that measure elements from Na up to U. When an X-ray photon enters the detector, it produces an electrical pulse with a height proportional to its energy. A multi channel analyzer counts the amplified pulses. The area of the peaks gives the intensity.

WDXRF includes gas-filled and scintillation detectors. The former measures from Be to Cu, and the latter measures from Cu to U. The height of the peak gives the intensity. In WDXRF, the majority of the power is dissipated as heat so it requires liquid cooling for the X-ray tube.[29]

2.5 | The fundamental coefficient method

The fundamental coefficient method is a combination between fundamental parameters and the statistical formulation of Lachance-Traill. This method addresses the difficulty of XRF to perform a precise matrix correction. The method requires standards and a series of calculations for the coefficients that must satisfy the Lachance-Traill equations and Tertian's identities. The theoretical parameters include mass absorption, excitation factors, and instrumental factors. Nowadays, all XRF software include such considerations. However, a specific method for the sample and calibration is still required.[30]

Thus, the effective coefficients for a given composition C_i, C_z,C_k, and so forth are as follows:

$$C_i = R_i(1 + \alpha_{iz}C_z + \alpha_{ik}C_k + \cdots) \quad (5)$$

where:

i represents a fluorescent element;

$C_{i,z,k\ldots}$ is the relative concentration of element i, z, $k\cdots$;

R_i is the relative intensity; and.

α_{iz}, α_{ik} $\cdots\cdots$ are the effective coefficients for the given composition C_i, C_k, and so forth.

The Tertian's identities are expressed by the following:

$$a_{ij} = \alpha'_{ij} - h_{ij}\frac{C_i}{R_i} \quad (6)$$

Followed by similar expressions for α_{ik}, α_{iz} $\cdots$.[30]

2.6 | Total reflection XRF (TXRF)

Total reflection X-ray fluorescence (TXRF) is used for the analysis of trace elements in small sample volumes, typically in the microlitre (μL) range. TXRF use the principle of total reflection of X-rays at a very shallow angle of incidence on a flat substrate. The incident X-rays excite the atoms, causing them to emit characteristic photons. These photons are then detected by a detector placed at a fixed angle.[31] The TXRF detects trace elements in the parts per billion (ppb, ng g^{-1}) range. It also offers excellent precision and accuracy, with relative standard deviations typically below 5%.

3 | APPLICATIONS

XRF is applied broadly in the sciences: 140 of the 250 WoS scientific categories cite it two times or more. Journals assigned to multidisciplinary materials science published 1510 of the 9000 published since 2018, and the other top categories are environmental sciences (1080 articles), multidisciplinary geosciences (930 articles), physical chemistry (884 articles), and then chemical engineering (717 articles). The journal *Fuel* in the chemical engineering category cites XRF most, with 81 articles. The other most prolific journals are *Journal of Environmental Chemical Engineering* (60), *Catalysis Today* (35), *Minerals Engineering* (33), *Energy & Fuels* (31), and *Desalination and Water Treatment* (30).

VOSViewer is a web-based software that generates maps of bibliographic data—keywords, authors, countries, and journals—from databases like Scopus and WoS. The keyword map for chemical engineering has four clusters of research centred on zeolite, catalyst, and mechanism with the most keywords, followed by temperature (T), combustion, pyrolysis, biomass, then adsorption (ads'n), kinetics, aqueous solution (aq sol'n), and finally oxidation (oxid'n), nanoparticles (NP), degradation. These clusters correlate broadly with the journals that publish the most work applying XRF: *Catalysis Today* belongs in the red cluster, *Fuel* and *Energy & Fuels* would be in the green cluster (Figure 11), *Desalination and Water Treatment* is in the blue cluster, while *Journal of Environmental Chemical Engineering* would belong in the yellow cluster. Although these journals have published the most with XRF, the top three cited articles are in *Applied Catalysis B-Environmental* and *Journal of Water Process Engineering*. The articles are entitled: "Enhanced photocatalytic removal of phenol from aqueous solutions using ZnO modified with Ag" (239 citations since 2018),[32] "Synthesis of CeaMnOx hollow microsphere with hierarchical structure and its excellent catalytic

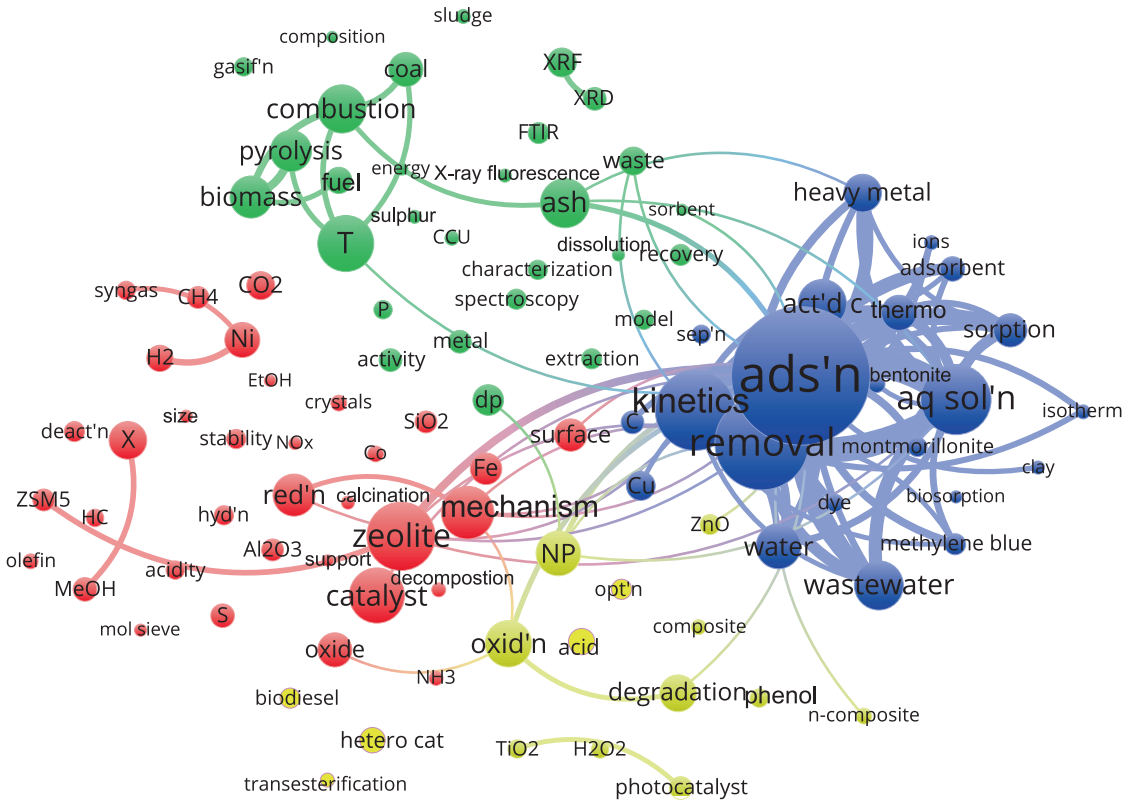

FIGURE 11 X-ray fluorescence bibliometric map of the 102 most cited keywords of articles from journals indexed by WoS from 2000 to 2022 in the chemical engineering category.[11,43] The size of each node and font-size correlate with the number of times the keywords occur in the database. ads'n is the largest node with 252 occurrences, and the smallest nodes correspond to 22 occurrences. The VOSViewer on-line software groups the keywords into four clusters: red cluster with 34 keywords, green (30), blue (22), and yellow (15). The largest nodes of each cluster are: zeolite (125 articles), *T* (102), ads'n (252), and oxid'n (86). The lines represent citation links. act'd c, activated carbon. ads'n, adsorption. aq sol'n, aqueous solution. CCU, carbon capture utilization. deact'n, deactivation. decomp'n, decomposition, EtOH, ethanol. gasif'n, gasification. HC, hydrocarbon. hetero cat, heterogeneous catalysis. hyd'n, hydrodynamics. MeOH, methanol. mol sieve, molecular sieve. n-composite, nano-composite. opt'n, optimization. oxid'n, oxidation. *P*, pressure. red'n, reduction. sep'n, separation. *T*, temperature. *X*, conversion.

performance for toluene combustion" (163 citations since 2019),[33] and "Development of synthetic zeolites from bio-slag for cesium adsorption: Kinetic, isotherm and thermodynamic studies" (147 citations since 2020).[34]

The *Can. J. Chem. Eng.* has published 10 articles that mention XRF since 2017. The major research themes have been $LiFePO_4$ and batteries,[35] metals,[36–38] sewage sludge[39] and adsorption, and bitumen,[40] bed coke,[41] and coal.[42]

XRF and X-ray spectroscopy is versatile non-destructive and for this reason it is applied in almost all human technological and research areas. Its practical industrial applications are often uncited, as they constitute a standard for steel alloy quality control, pharmaceuticals to assess potential contamination, and petroleum to measure sulphur and metal content in crude oil and lubricants. More recent applications could be directed at measuring the capability of regenerated biochar at removing Hg.[44] In archeology, it is used to determine silver content, and its evolution over time, in ancient coins like for Greek coins in a small colony on the Iberian Peninsula minted from 4 to 1 B.C.[45] This technique can be used to determine different alloy grades such as gold purity in jewellery,[46] and to determine heavy metals presence in medicinal plants, cosmetics, and ethnic spices.[47,48] Soil pollution is commonly analyzed using portable and desktop XRF.[49]

Archaeology: Researchers analyze silver content in coins, coatings, and other objects with XRF. In geoarchaeology they examine target compounds like basalt in artefacts. The trace compounds detected by XRF relate to the artefacts' origins.[50]

Environment: XRF detects pollutants in various environments like soils, waste, materials, and sediments, like those near a crude oil facilities in the Niger Delta.[51]

Medicine: XRF is used for the detection of elements in blood, heavy metals in tattoo ink, and non-radioactive iodine assimilation.[52]

Industry: Industrially, XRF determines the compositions of minerals and rock. It measures the

concentration of P, S, Cl, K, and Ca in phosphate rock, for example, which is necessary for phosphate processing.[53] XRF was used to determine potassium content of illite in Canadian oil sands. It proved more reliable with a better tolerance to surface contamination compared with other techniques such as methylene blue titration.[54]

In the chemical engineering research, we apply the technique to determine the success of slime coal particle separation and then to validate a computational fluid dynamics (CFD) method (green cluster).[42] XRF also determined the copper content after a novel bioleaching process to selectively recover precious metals from waste of electrical and electronic equipment (WEEE) (blue cluster).[37] These examples demonstrate the reach and versatility of the XRF spectroscopy technique.

4 | UNCERTAINTY AND ERRORS

Portable XRF (PXRF) units are popular because they cost less then desktop units and are easy to transport from one site to another. However, laboratory/desktop XRF instruments detect more elements than portable systems (Na to U) and are more precise and accurate. Industries and miners apply PXRF mostly for qualitative analysis (blue cluster).[55]

4.1 | Error sources and limitations

Limitations of XRF include the following:

1. Interference effect: Interference errors are linked to the background and other characteristic emissions lines. Background interference can be removed by a fine measuring of the background and subtracting it from the measurement. This is especially critical when background peaks are close to the elements in the sample.[56]

   Spectral interference—overlapping fluorescent (emission) lines. The tail of one peak overlaps the centre of an adjacent element to increase the intensity of this peak, which then overestimates the concentration. To account for this phenomenon requires standards to determine the real element contribution. Alternatively, we use secondary emission lines on the spectrum where there is no overlap.[56,57]

2. Matrix effect: The intensity of the emission line depends on the composition and morphology of the sample, which compromises the relationship between fluorescence X-ray and concentration:[56,58]

   a. Absorption effect: Fluorescent photons are partially absorbed by the sample before reaching the detector. This underestimates element concentration because it attenuates the signal intensity.
   b. Enhancement effect: Contrary to the absorption effect, fluorescent photons from the sample excite other elements, increasing X-ray emission. This overestimates concentration.[56]

   We mitigate the matrix effect with calibration, mathematical models, or introducing empirical values.[58–60] Usually, XRF software corrects for these, but require data.

3. Depth resolution: While it is possible to increase X-ray penetration by increasing the beam energy, different atoms will return fluorescent X-ray at different depths. Silica will only return photons from 20 pm, while zirconium fluoresces from 3.4 mm Therefore, some elements are more identifiable at low concentrations.[61]

   Penetration depth, x, varies with the the following[61]:

$$x = -\ln \frac{I}{I_0}\left(\frac{\rho}{\mu}\right) \tag{7}$$

   where I is the intensity of photons returning from the sample, I_0 is the number of photons entering the sample, $\frac{\mu}{\rho}$ is the mass attenuation coefficient of a given element for a particular matrix, and ρ is the object density (Figures 12 and 13).

4. Sensitivity: Factors that limit sensitivity include sample composition, sample preparation, and conditions of measurement. It is defined by the number of photons counted by the detector versus the number of photons that pass through it. Thin detectors might allow the photons to pass without triggering a signal. In the range of the X-rays, the photo-effect predominates with respect to photon detection, and thus a 10 mm thickness for the scintillator is sufficient.

5. Lowest limit of detection: X-rays generated and detected are random and the the intensity depends on the dwell time, and so follow a statistical distribution forming a Gaussian distribution.

XRF is a mass analyzer and requires a substantial sample: diameter above 10 mm thickness greater than

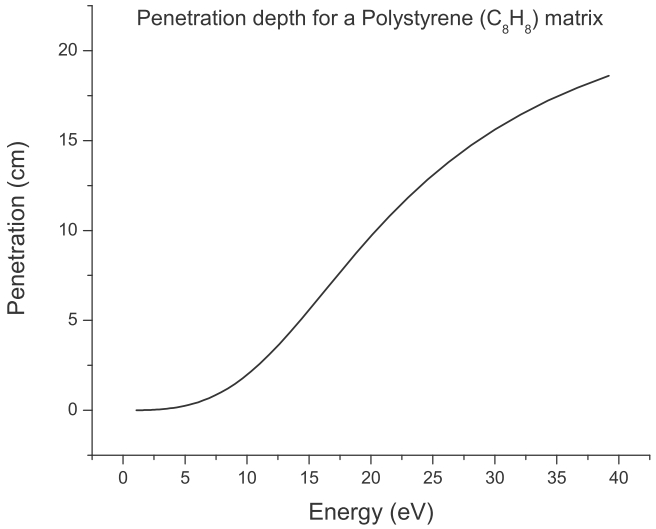

FIGURE 12 X-ray penetration in a polystyrene C_8H_8 (PS) matrix assuming a density of 1.04 g cm^{-3}. Photons penetration at 40 kV reach 200 mm.

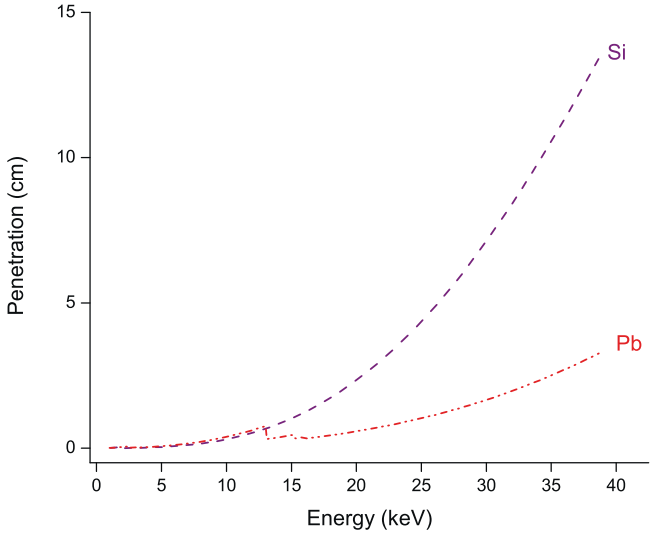

FIGURE 13 X-ray penetration comparison between Si and Pb.

2.5 mm for ED-XRF.[50] For smaller samples, laser ablated inductively coupled plasma spectrometry (LA-ICP-MS) is better suited. LC, LD and LQ are the symbols to represent critical level, detection limit, and determination limit, respectively (Table 4).[63] The sample depth depends on the incident radiation and the element of interest (Table 5).

5 | EXPERIMENTAL PROCEDURE

1. Sample preparation: This is a critical step as it impacts both accuracy and precision.[64] The size and shape of the sample depends on the instrument being used.

TABLE 4 International recommendations and nomenclature on analytical detection and quantification on concepts.[62]

Concept	Symbol	Definition
Critical Level	LC	The minimum signal which an instrument may reliably recognized as 'detected'
Detection Limit	LD	The net signal level that can be expected to lead to detection
Determination Limit	LQ	The signal level over which the signal could be quantified

Abbreviations: LC, critical level; LD, detection limit; LQ, determination limit.

TABLE 5 Analysis depth.

Material	Mg Kα µm	Cr Kα	Sn Kα
Lead	0.7	4.5	55
Iron	1	35	290
SiO_2	8	110	9000
$Li_2B_4O_7$	13	900	46,000
H_2O	16	1000	53,000

2. Instrument setup: Set the measurement conditions, such as known element present in the sample, elements that are absent, voltage, filters, sample mass, dimensions when possible, and measurement time. A calibration might be needed occasionally to improve sensitivity together with an element library, which is usually included with the instrument.
3. Sample analysis: The samples is then placed in the instrument according to the sample preparation and analysis method selected. A safety procedure to ensure that the XRF analysis chamber is well closed is recommended (usually the instrument has safety protocols).
4. Data analysis: The results reported by the instrument software.
5. Quality control: We recommend repeating the measurements multiple times to evaluate the repeatability. Introducing standards to calibrate the signal increases the confidence in the accuracy.

5.1 | Sample preparation

A sample diameter greater than 10 mm and thicker than 2.5 mm are optimal for ED-XRF analyses.[50] An accurate analysis requires a sample surface layer that is homogeneous and representative of the bulk sample. For solid samples or metals that are coated or oxidized in air, grinding and polishing removes the rust and coating

layers. For powders, both a supporting film to place under the sample or pressing the sample into a tablet works well.

5.2 | Case of study

In the plastic industry, XRF has several advantages:

1. It identifies elemental composition rapidly (from seconds to minutes) and accurately quantifies elemental composition of contaminants and additives such as pigments, fillers, stabilizers, or flame retardants for quality control and environmental compliance.[65]
2. It is a non-destructive technique so we can apply other spectroscopic or mechanical measurements, which is particularly important for research when only small quantities are available and for expensive or irreplaceable parts.[66]
3. Its high sensitivity and accuracy in determining concentrations of trace elements—impurities or contaminants—to evaluate their impact on material properties and quality.[67].
4. Compared to most other methods (like mass spectrometry), it is cost effective, more accessible to a wider range of users, and apt for quality control with frequent analyses.

Plastic pollution and its impact on the environment is a growing concern as micro-plastics form when it degrades. Besides the increase in micro-plastics in bodies of water, additives are also a concern. Brominated fire retardant additives (BFRs) (piolybrominated diphebyl ethers [PBDEs] and polybrominated byphenyls [PBBs]) were the preferred class of compounds to meet fire safety norms for electric and electronic plastics. These fire retardants are currently banned because of their impact on the environment and their health hazards—endocrine disruption, neurotoxicity, and developmental toxicity.[68–72] As of 21 July 2023, Australian authorities require importers to apply for a special authorization to import decabromodiphenyl ether (decaBDE).[73] These compounds limit recyclability. Companies that want to use WEEE plastics as a feed-stock for, among others, recycling or waste-to-energy must remove BFRs. XRF instruments are a prime means to pre-sort polymers to minimize contamination. However, companies must certify material composition with more detailed analyses (Gas chromatography–mass spectrometry [GC–MS], for example) of the extracted BFRs to meet international norms like IEC 62321–6.

As part of the project to debrominate electronic plastics, we analyzed several waste samples. The analyses detected Br and other elements in the plastics of WEEE devices (Table 6) with Br concentrations reaching 10% of the total mass and Sb up 0.5%. The accuracy of the measurement is quite good with a standard deviation of $<0.1\ \%$ of the Br and high concentration and $<5\ \%$ for the all the other elements except Ni. The distribution of Br in the sample varies by 40%! Industry detects bromine in plastics with XRF guns and the results are comparable to GC–MS.[74] XRF and XRF guns have many advantages compared to GC such as portability, speed, and ease of sample preparation. However, matrix effects and peak overlapping compromise accuracy when neglected. The type of sample and its preparation is a key factor to maximize the repeatability. In 7, we demonstrated the accuracy and reliability of XRF guns to analyze polymers, and for this reason industry uses the instrument so readily. We do, however, recommend repeating measurements as many as five times, and as demonstrated above, when the elements are distributed unevenly, multiple samples must be taken from different areas to ensure that it is representative of the whole piece (Table 6): the standard deviation of the Br measurement was less than 1% but differences between samples from different areas of the piece were up to 40,000 ppm The heterogeneous distribution could also be due to the manufacturing.

Here, we compare the concentration of 10 samples from a Bruker S1 TITANXRF gun with a neutron activation analysis (NAA) (Table 7). Although the standard deviation of the error is 22%, the range of concentration varies over four orders of magnitude (10 to $>100\ 000$). Presumably, the NAA data best represent the actual concentration of BFR in the sample, so the gun overestimates the true value.

XRF produces both qualitative and quantitative data. Quantitative analyses require mass, density, suspected elements in the sample, dwell time, and calibration standards for the software. The elemental concentration is ultimately calculated statistically based on both measurement and input parameters. Qualitative analyses require less input data and report sample composition to a lesser degree of accuracy. XRF qualitative analyses are fast and relativity easy to interpret.[58] The spectra present a series of peaks representing the detected photons per second (cps) at a specific energy (y-axis represents intensity, whereas x-axis is energy).

The Br KA peak height of a WEEE plastic approaches 10,000 cps before treatment (Figure 14 left panel). After the debromination treatment of these end-of-life plastics, the Br KA peak virtually disappeared, barely reaching 12 cps (Figure 14 right panel). With this spectrum, we deduce that that the treatment method is very efficient, although we are incapable of assigning a final Br

TABLE 6 X-ray fluorescence elemental analyses of a waste of electrical and electronic equipment (WEEE) high impact polystyrene (HIPS) sample (PS-FR(17) code). Note the very high concentration of Br and Sb. Each of the four rows of data are XRF measurements from different pieces of the same WEEE plastic part that had been ground down For each row represents at least four measurements to calculate $\pm s$ ($n \geq 4$).

Ca		Fe		Ni		Zn		Se		Br		Sb	
ppm	±	ppm	±	ppm	±	ppm	±	ppm	±	ppm	±	ppm	±
241	8	91	5	10	9	96	3	190	4	62,000	46	2800	6
205	2.2	24	1.4	< LOD	1	100	3	230	5	100,000	74	5000	7
247	8	164	7	16	6	112	4	150	4	77,000	62	3300	7
189	6	19	4	9	5	122	4	340	5	76,000	69	5100	9

Abbreviation: ppm, parts per million which equals to mg/kg.

TABLE 7 A validation table comparing the bromine concentration measured by a Bruker X-ray fluorescence TITAN S1 gun and neutron activation analysis (NAA) (Slowpoke reactor at Polytechnique Montreal).

Sample	m(g)	x_{Bruker} (μg g^{-1})	x_{NAA}(μg g^{-1})	% error $\frac{x_{\text{Bruker}}-x_{\text{NAA}}}{(x_{\text{Bruker}}+x_{\text{NAA}})/2}$
1	0.55	282	208	30%
2	0.68	61	36	51%
3	0.41	20	20.5	-2%
4	0.91	92,000	97,400	−6%
5	0.68	100,000	93,000	7%
6	0.39	32	17	62%
7	0.64	392	333	16%
8	0.59	113,000	99,000	13%
9	0.39	140,000	94,500	39%
10	0.27	119,000	97,800	20%

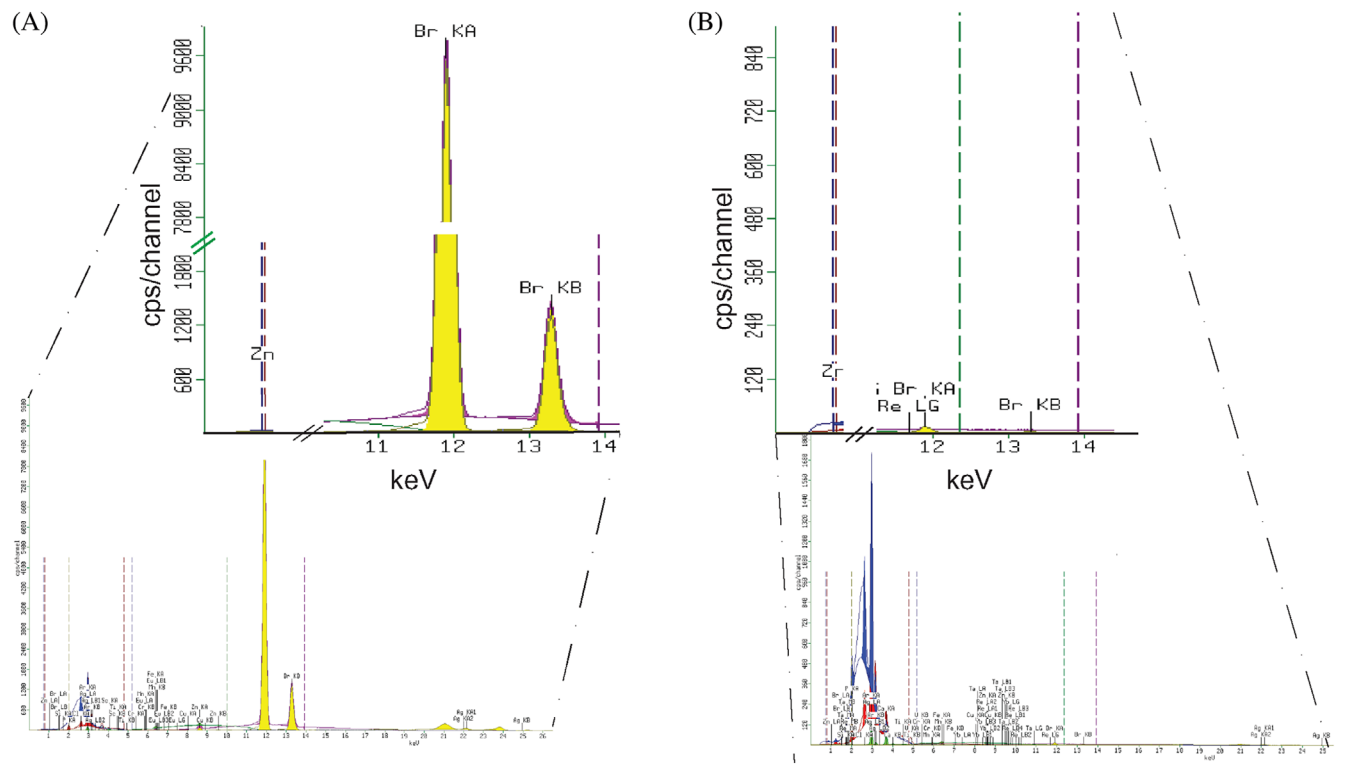

FIGURE 14 X-ray fluorescence results from a plastic sample containing brominated fire retardant before and after treatment. The peak difference relative to the bromine energy lines at 12 kV are clearly evident.

concentration or the scavenging efficiency as it is only a qualitative analysis. This approach is suitable to quickly determine some results, or to find elements and their relative abundance in the sample when the sample's composition is unknown.

6 | CONCLUSIONS

XRF spectroscopy detects species composition from concentrations of 1 ppm to 100% of any element from Na to U, without destroying the sample. Portable XRF guns are versatile and report Br concentration within about 25% of neutron activation analysis. To achieve higher accuracy requires a detailed calibration with a precise sample preparation procedure, which depends on the matrix, the elements of interest, and the sample state (solid, liquid, powder···). Furthermore, quantitative analyses require some knowledge of the sample to be able to account for the limitations of the technique. However, even without prior knowledge of the sample composition, XRF analysis is capable of qualitative analysis. Many instruments, like the Epsilon 4 from Malvern Panalytical, come with a pre-calibration routine for all elements that facilitates quantitative analysis.

AUTHOR CONTRIBUTIONS

Mario Ferreiro González: Conceptualization; data curation; formal analysis; visualization; writing – original draft; investigation; methodology; writing – review and editing; validation. **Nooshin Saadatkhah:** Conceptualization; data curation; formal analysis; visualization; writing – original draft; methodology; supervision; investigation; writing – review and editing; validation. **Gregory S. Patience:** Visualization; writing – original draft; methodology; investigation; supervision; project administration; writing – review and editing; validation; funding acquisition; resources.

PEER REVIEW

The peer review history for this article is available at https://www.webofscience.com/api/gateway/wos/peer-review/10.1002/cjce.25218.

DATA AVAILABILITY STATEMENT

The data that support the findings of this study are available from the corresponding author upon reasonable request.

ORCID

Gregory S. Patience https://orcid.org/0000-0001-6593-7986

REFERENCES

[1] A. S. Panchbhai, *Journal of Indian Academy of Oral Medicine and Radiology* **2015**, *27*, 90.
[2] A. Iglesias-Juez, G. L. Chiarello, G. S. Patience, M. O. Guerrero-Pérez, *Can. J. Chem. Eng.* **2022**, *100*, 3.
[3] G. E. Smith, J. Z. Buchwald, A. Warwick Eds., *Histories of the Electron: The Birth of Microphysics*, Vol. 1, Springer-Verlag, New York **2001**, p. 21.
[4] I. W. Griffiths, *Rapid Commun. Mass Spectrom.* **1997**, *11*, 2.
[5] C. G. Barkla, *Dublin Philos. Mag. J. Sci.* **1911**, *22*, 396.
[6] J. E. Brittain, *IEEE Industry Applications Magazine* **2004**, *10*, 9.
[7] R. G. Egdell, E. Bruton, *Philos. Trans. R. Soc., A* **2020**, *378*, 20190302.
[8] H. G. J. Moseley, *Dublin Philos. Mag. J. Sci.* **1913**, *26*, 1024.
[9] D. Coster, R. D. L. Kronig, *Physica* **1935**, *2*, 13.
[10] R. Glocker, H. Schreiber, *Ann. Phys.* **1928**, *390*, 1089.
[11] Web of Science™ Core Collection. **2023** http://apps.webofknowledge.com (accessed: July 2023).
[12] J. Lefebvre, F. Galli, C. L. Bianchi, G. S. Patience, D. C. Boffito, *Can. J. Chem. Eng.* **2019**, *97*, 2588.
[13] H. Khan, A. S. Yerramilli, A. D'Oliveira, T. L. Alford, G. S. P. Daria, C. Boffito, *Can. J. Chem. Eng.* **2020**, *98*, 1255.
[14] M. O. Guerrero-Pérez, G. S. Patience, *Can. J. Chem. Eng.* **2020**, *98*, 25.
[15] G. S. Patience, *Can. J. Chem. Eng.* **2018**, *96*, 2312.
[16] N. Braidy, A. Béchu, J. C. de Souza Terra, G. S. Patience, *Can. J. Chem. Eng.* **2020**, *99*, 628.
[17] R. Klockenkamper, A. Von Bohlen, *Bohlen* Total-Reflection X-Ray Fluorescence Analysis and Related Methods, John Wiley & Sons, Hoboken, NJ **2014**.
[18] R. V. Murphy, H. Maharaj, J. Lachapelle, P. K. Yuen, *Operator of Portable X-Ray Fluorescence Analyzers (XRF) Certification Information and Examination Preparation*, 4th ed., Natural Canada Resources, Nepean, Canada **2017**.
[19] M. Hall, A. Hunt Eds., *The Oxford Handbook of Archaeological Ceramic Analysis*, Oxford University Press, Oxford **2016**, p. 341.
[20] J. H. Hubbell, S. M. Seltzer, *Seltzer* Tables of X-Ray Mass Attenuation Coefficients and Mass Energy-Absorption Coefficients 1 keV to 20 MeV for Elements Z = 1 to 92 and 48 Additional Substances of Dosimetric Interest, National Institute of Standards and Technology, Gaithersburg, MD **1995**.
[21] B. Beckhoff, B. Kanngiesser, N. Langhoff, R. Wedell, H. Wolff, *Handbook of Practical X-Ray Fluorescence Analysis*, Springer, Berlin, Heidelberg, Berlin **2007**.
[22] N. Hooshang, U. Sotaro, E. Dimitris, *Interaction of Radiation with Matter*, CRC Press, New York **2012**.
[23] W. D. Coolidge, *US Patent 1,946,312*. **1934**.
[24] K. Ono, T. Sakuma, H. Takahashi, *US Patent 4,730,353*. **1988**.
[25] D. S. Lee, T. C. T. Jr, *US Patent 5,008,918*. **1991**.
[26] J. M. Boone, T. R. Fewell, R. J. Jennings, *Med. Phys.* **1997**, *24*, 1863.
[27] A. K. Gupta, *International Journal of Core Engineering and Management* **2014**, *1*, 36.
[28] E. T. Puusaari, *US Patent 7,203,283*. **2007**.
[29] J. M. Guthrie, J. R. Ferguson, *Archaeometry Laboratory at the University of Missouri Research Reactor* **2012**, https://archaeometry.missouri.edu/xrf_technical.html (accessed: April 2023).

[30] N. Broll, *X-Ray Spectrom.* **1986**, *15*, 271.
[31] P. Wobrauschek, *X-Ray Spectrom.* **2016**, *36*, 289.
[32] V. Vaiano, M. Matarangolo, J. Murcia, H. Rojas, J. Navio, M. Hidalgo, *Appl. Catal., B* **2018**, *225*, 197.
[33] L. Zhao, Z. Zhang, Y. Li, X. Leng, T. Zhang, F. Yuan, X. Niu, Y. Zhu, *Appl. Catal., B* **2019**, *245*, 502.
[34] S. Khandaker, Y. Toyohara, G. C. Saha, M. R. Awual, T. Kuba, *Journal of Water Process Engineering* **2020**, *33*, 101055.
[35] Y. Liu, B. M. Norouzi, X. Wei, L. Ruying, W. Zhiqiang, R. Steeve, S. Pierre, D. Mickaël, L. Guoxian, S. Tsun-Kong, S. Xueliang, *Can. J. Chem. Eng.* **2019**, *97*, 2218.
[36] L. Sun, S. Xin, L. Kai, W. Chi, S. Xin, N. Ping, H. Haibao, *Can. J. Chem. Eng.* **2020**, *98*, 1534.
[37] S. K. Utimura, S. J. Arevalo, C. G. A. Rosario, M. Q. Aguilar, J. A. S. Tenório, D. C. R. Espinosa, *Can. J. Chem. Eng.* **2019**, *97*, 2920.
[38] K. John, B. Musamba, *Can. J. Chem. Eng.* **2021**, *99*, 896.
[39] P. F. P. Nascimento, J. F. Sousa, J. A. Oliveira, R. D. Possa, F. C. Carvalho, J. A. C. Ruiz, M. M. Pedroza, M. B. D. Bezerra, *Can. J. Chem. Eng.* **2017**, *95*, 2148.
[40] Q. Lian, Z. U. Ahmad, D. D. Gang, M. E. Zappi, D. L. B. Fortela, R. Hernandez, *Chemosphere* **2020**, *248*, 126078.
[41] L. Zhihong, D. Boyu, L. Qingsong, J. Yan, L. Zuian, Y. Hairui, Z. Man, *Can. J. Chem. Eng.* **2023**, *101*, 2526.
[42] C. Sheng, C. Duan, Y. Zhao, C. Zhou, Y. Zhang, *Can. J. Chem. Eng.* **2017**, *95*, 2129.
[43] N. J. van Eck, L. Waltman, *Scientometrics* **2010**, *84*, 523.
[44] L. Jia, P. Cheng, Y. Yu, S. H. Chen, C. X. Wang, L. He, H. T. Nie, J. C. Wang, J. C. Zhang, B. G. Fan, Y. Jin, *J. Environ. Manage.* **2023**, *326*, 116790.
[45] A. Pitarch, I. Queralt, *Nucl. Instrum. Methods Phys. Res., Sect. B* **2010**, *268*, 1682.
[46] A. Marucco, *Nucl. Instrum. Methods Phys. Res., Sect. B* **2004**, *213*, 486.
[47] I. Queralt, M. Ovejero, M. Carvalho, A. Marques, J. Llabrés, *X-Ray Spectrom.* **2005**, *34*, 213.
[48] K. G. McIntosh, D. Guimarães, M. J. Cusack, A. Vershinin, Z. Chen, K. Yang, P. J. Parsons, *Int. J. Environ. Anal. Chem.* **2016**, *96*, 15.
[49] A. G. Caporale, P. Adamo, F. Capozzi, G. Langella, F. Terribile, S. Vingiani, *Sci. Total Environ.* **2018**, *643*, 516.
[50] M. K. Davis, T. L. Jackson, M. S. Shackley, T. Teague, J. H. Hampel, M. S. Shackley Eds., *X-Ray Fluorescence Spectrometry (XRF) in Geoarchaeology*, Springer, New York **2011**, p. 45.
[51] E. I. Obiajunwa, D. A. Pelemo, S. A. Owolabi, M. K. Fasasi, F. O. Johnson-Fatokun, *Nucl. Instrum. Methods Phys. Res., Sect. B* **2002**, *194*, 61.
[52] D. Bazin, E. Foy, S. Reguer, S. Rouziére, B. Fayard, H. Colboc, J.-P. Haymann, M. Daudon, C. Mocuta, *C. R. Chim.* **2022**, *25*, 165.
[53] J. Hasikova, A. Sokolov, V. Titov, A. Dirba, *Procedia Eng.* **2014**, *83*, 455.
[54] A. Li, Z. Xu, *Can. J. Chem. Eng.* **2020**, *98*, 360.
[55] M. S. Shackley, *The Encyclopedia of Archaeological Sciences*, John Wiley & Sons, Ltd, Hoboken, NJ, **2018**, p. 1.
[56] K. Andrzej, R. Zofia, S. Marek, *X-Ray Spectrom.* **1982**, *11*, 135.
[57] K. Norrish, B. W. Chappell, J. Zussman Eds., *Physical Methods in Determinative Mineralogy*, Academic Press, London **1977**, p. 201.
[58] A. D. Karathanasis, B. F. Hajek, *Methods of Soil Analysis*, John Wiley & Sons, Hoboken, NJ **1996**, p. 161.
[59] M. Wang, Y. Gu, H. Lu, L. Ge, Q. Zhang, G. Zeng, *Spectrochim. Acta, Part A* **2022**, *193*, 106438.
[60] J. Lu, G. Jinke, W. Qiaoqiao, X. Tang, L. Tian, H. Yaru, Z. Xinyun, *Appl. Sci.* **2022**, *12*, 568.
[61] D. B. Lee, B. L. MacDonald, *Advances in Portable X-Ray Fluorescence Spectrometry: Instrumentation, Application and Interpretation*, 1st ed., Royal Society of Chemistry, London **2022**.
[62] L. A. Currie, *Anal. Chem.* **1968**, *40*, 586.
[63] L. N. Rand, *PhD Thesis*, Colorado School of Mines. Arthur Lakes Library (llinois, CO) **2019**.
[64] N. K. Aylikci, O. Oruc, E. Bahceci, A. Kahoul, T. Depci, V. Aylikci, *X-Ray Fluorescence in Biological Sciences*, John Wiley & Sons, Hoboken, NJ **2022**, p. 91.
[65] N. Marijan, K. Peter, Z. Maja, *X-Ray Spectrom.* **2012**, *41*, 87.
[66] O. Akira, G. P. Pereira, S. Christian, R. Zsolt, *J. Compos. Sci.* **2019**, *3*, 54.
[67] A. N. Kadachi, M. A. Al-Eshaikh, *X-Ray Spectrom.* **2012**, *41*, 350.
[68] L. S. Birnbaum, D. F. Staskal, *Environ. Health Perspect.* **2004**, *112*, 9.
[69] The European Parliament and The Council of the European Union, *Official Journal of the European Union* **2003**, 42, https://eur-lex.europa.eu/LexUriServ/LexUriServ.do?uri=OJ:L:2003:042:0045:0046:EN:PDF (accessed: July 2023).
[70] U. E. P. Agency, Toxic Substances Control Act (TSCA) Chemical Substance Inventory: Revised Inventory Notice, https://www.epa.gov/tsca-inventory/abouttsca-chemical-substance-inventory (accessed: July 2021).
[71] State of California Department of Toxic Substances Control, Priority Product Work Plan: 2018–2020 **2017**, https://dtsc.ca.gov/wp-content/uploads/sites/31/2018/10/Final_2018-2020_Priority_Product_Work_Plan.pdf (accessed: July 2023).
[72] Department of Health and Care, Australia, Decabromodiphenylethane Regulatory Action. www.industrialchemicals.gov.au/news-andnotices/decabromodiphenylethane-regulatory-action (accessed: July 2023).
[73] Department of Health and Care, Australia, Decabromodiphenylethane (DecaBDE) and Perfluorooctanoic Acid (PFOA)-Related Compounds: Authorisation Required. https://www.industrialchemicals.gov.au/news-andnotices/decabde-and-pfoa-related-compoundsauthorisation-required-21-july-2023 (accessed: July 2023).
[74] A. Aldrian, A. Ledersteger, R. Pomberger, *Waste Manage.* **2015**, *36*, 297.

How to cite this article: M. F. González, N. Saadatkhah, G. S. Patience, *Can. J. Chem. Eng.* **2024**, 1. https://doi.org/10.1002/cjce.25218